Bioactive Materials 6 (2021) 361–374

Contents lists available at ScienceDirect

Bioactive Materials

journal homepage: http://www.keaipublishing.com/biomat

Conditioned medium-electrospun fiber biomaterials for skin regeneration

Lu Chen[a,1], Liying Cheng[a,1], Zhen Wang[b], Jianming Zhang[c], Xiyuan Mao[a], Zhimo Liu[a], Yuguang Zhang[a], Wenguo Cui[b], Xiaoming Sun[a,*]

[a] Department of Plastic and Reconstructive Surgery, Shanghai Ninth People's Hospital, Shanghai Jiao Tong University School of Medicine, 639 Zhi Zao Ju Road, Shanghai, 200011, PR China
[b] Shanghai Key Laboratory for Prevention and Treatment of Bone and Joint Diseases, Shanghai Institute of Traumatology and Orthopaedics, Ruijin Hospital, Shanghai Jiao Tong University School of Medicine, 197 Ruijin 2nd Road, Shanghai, 200025, PR China
[c] National Research Center for Translational Medicine, Ruijin Hospital, Shanghai JiaoTong University School of Medicine, Shanghai, PR China

ARTICLE INFO

Keywords:
Conditioned medium
Biomaterials
Regenerative medicine
Skin regeneration
Electrospun fiber

ABSTRACT

Conditioned medium (CM) contains variety of factors secreted by cells, which directly regulate cellular processes, showing tremendous potential in regenerative medicine. Here, for the first time, we proposed a novel regenerative therapy mediated by biodegradable micro-nano electrospun fibers loaded with highly active conditioned medium of adipose-derived stem cells (ADSC-CM). ADSC-CM was successfully loaded into the nanofibers with biological protection and controllable sustained-release properties by emulsion electrospinning and protein freeze-drying technologies. *In vitro*, ADSC-CM released by the fibers accelerated the migration rate of fibroblasts; inhibited the over proliferation of fibroblasts by inducing apoptosis and damaging cell membrane; in addition, ADSC-CM inhibited the transformation of fibroblasts into myofibroblasts and suppressed excessive production of extracellular matrix (ECM). *In vivo*, the application of CM-biomaterials significantly accelerated wound closure and improved regeneration outcome, showing superior pro-regenerative performance. This study pioneered the application of CM-biomaterials in regenerative medicine, and confirmed the practicability and significant biological effects of this innovative biomaterials.

1. Introduction

The use of mesenchymal stem cells (MSCs) based biomaterials represents and remains an attractive strategy for tissue engineering applied to skin regeneration [1,2]. With the support and regulation of biomaterial scaffolds on stem cells, MSCs transdifferentiate into epidermal and dermal cells, and further exert anti-inflammatory, immunemodulative, anti-scarring and antimicrobial properties, significantly improving damaged skin repair [3–7]. Although MSCs-based biomaterials have made great progress in skin regeneration, there are still many limitations: (1) immune rejection [8]; (2) low cell survival rate [9]; (3) uncontrolled cell differentiation [10]; and (4) potential cancer formation [11]. These defects seriously hinder further researches and clinical application of MSCs-based biomaterials.

The therapeutic effects of MSCs are generally mediated by various secreted cytokines [12], growth factors [13], extracellular matrix (ECM) proteins [14] and different types of extracellular vesicles [15]. Conditioned medium of MSCs (MSC-CM) containing these secreted factors directly addresses the limitations associated with above mentioned MSCs-based therapy and has been demonstrated to be an effective cell-free medicinal product for skin regeneration. For example, JiaYang et al. found that MSC-CM significantly promoted angiogenesis and accelerated wound closure without obvious scar formation [16]. Further, Kim et al. demonstrated that the accelerated migration of human keratinocytes and fibroblasts was tightly associated with Galectin-1 from MSC-CM [17]. And Eun et al. revealed that factors contained in MSC-CM enhances wound healing by activating TGF-β/SMAD2 and PI3K/AKT pathways [18]. Although MSC-CM was proven to be reliable regenerative medicine for skin regeneration, due to bioactive components' structural instability, unpredictable biological distribution, and the systemic clearance *in vivo*, it is difficult to ensure the direct use effect of conditioned medium (CM). Therefore, to construct an effective CM delivery system, keep the structural integrity and biological function stability of bioactive substances, make them long-term controllably release, and maintain effective therapeutic concentration during the whole process of tissue healing is the key to

Peer review under responsibility of KeAi Communications Co., Ltd.
* Corresponding author.
E-mail address: drsunxm@126.com (X. Sun).
[1] These authors contributed equally to this work.

https://doi.org/10.1016/j.bioactmat.2020.08.022
Received 8 May 2020; Received in revised form 13 August 2020; Accepted 22 August 2020

promoting skin regeneration.

To assist the fast healing of skin wounds, dermal scaffolds have been engineered to provide an efficient cover of the wounds and protect the body temporarily yet supporting cellular ingrowth and tissue regeneration [19]. Among the existing scaffolds, electrospun fibrous scaffolds are constituted by continuous fibers with diameters ranging from several micrometers down to a few nanometers and architecturally similar to the nature structure of ECM [20]. The scaffolds assess an extremely high surface-to-volume ratio to allow cell attachment and contain microscale interconnected pores, which are essential to transport the oxygen and nutrient supply for cell growth [21]. In addition to structural advantages, the development of electrospinning technology has made the electrospun fibrous scaffolds more closely mimic ECM functionally [22,23]. Notably, emulsion electrospinning developed recently was adopted to prepare protein loaded fibers with integral core-sheath structure, which was essential for electrospun fibers to increase the encapsulation efficiency, retard the initial burst release, and long-term maintain the bioactivities [24,25]. Therefore, the electrospun fibrous scaffolds formed by emulsion electrospinning seems to be an ideal carrier of MSC-CM for further clinical application.

Adipose-derived stem cell (ADSC) is a commonly used pro-repair MSC in regenerative medicine. Here, inspired by the pro-regenerative properties of conditioned medium of ADSCs (ADSC-CM) and the structural and functional advantages of electrospun fibrous scaffolds formed by emulsion electrospinning, an ADSC-CM loaded micro-nano polylactic acid (PLA) electrospun fiber (MPF@CM) was developed (Fig. 1a). The unique core-shell structure of the micro-nano electrospun fibers with hyaluronic acid (HA) nanoparticles inside effectively protected the structural integrity and bioactivity of encapsulated factors and maintained sustained release behavior. With the degradation of materials, ADSC-CM gradually released and acted on fibroblasts within the wound. On the one hand, it accelerated wound healing by promoting the migration of fibroblasts; on the other hand, it inhibited scar formation by limiting excessive production of ECM, thus promoting skin regeneration (Fig. 1b). Therefore, a novel CM-biomaterial with simple preparation process, no immune rejection, and significant therapeutic efficacy was proposed, showing great potential for further clinical applications.

2. Material and methods

2.1. ADSCs isolation

Human subcutaneous adipose tissue samples were acquired from cosmetic liposuction (Plastic and Reconstructive Surgery Department of Shanghai Ninth People's Hospital, Shanghai Jiao Tong University School of Medicine) of healthy females (mean age, 31 years; range, 20–35 years) with informed consents as approved by the institutional review boards.

Systems that isolate ADSCs have found clinical application in different fields. Of all the methods for obtaining ADSCs, enzyme digestion is the most commonly used. ADSCs were isolated according to the method described by Araña M et al. [26]. Briefly, collected adipose tissue was digested with 0.2% Collagenase type I (Gibco, USA), shaking at 37 °C for 1 h. Digested tissue was filtered and centrifuged at 600 × *g* for 5 min. Collected cells were resuspended and cultured in DMEM (Gibco, USA) supplemented with 10% FBS (Gibco, USA) and 100 units/mL of penicillin, 100 mg/mL of streptomycin (Gibco, USA) at 37 °C in a humidified incubator with 5% CO_2. The resulting cell population was maintained over 3–5 days until confluence, which were represented as passage 1. ADSCs were cultured and expanded in control medium, and used for the experiments at passage 3. As a kind of mesenchymal stem cells, ADSCs theoretically express typical marker profile and have multi-directional differentiation potential in common with other mesenchymal stem cells. Thus, here we identified the surface markers of these cells obtained (CD31, CD34, CD45, CD29, CD90, CD105) and performed induced osteogenic differentiation and induced adipogenic differentiation to verify these cells obtained were ADSCs (Appendix B).

2.2. Acquisition of hypertrophic scar fibroblasts (HSFs)

Hypertrophic scar (HS) specimens obtained from the patients (2 males and 1 female) (mean age, 23 years; range, 16–32 years) of Plastic and Reconstructive Surgery Department of Shanghai Ninth People's Hospital signing informed consent during operation were used to obtain HSFs, which has been described previously [27]. Briefly, tissues were rinsed with PBS three times after removing excessive adipose. Next, tissues were sectioned into small pieces and incubated in 0.3% collagenase NB4 (SERVA, Heidelberg, Germany) at 37 °C for 4 h. The isolated fibroblasts were subsequently cultured. They were used in this experiment at passage 3.

2.3. Collection and lyophilization of ADSC-CM

ADSCs (3×10^5 cells) of passage 3 were seeded on a 100 mm dish and cultured until 90% confluence. Then a serum free medium was added to replace the growth medium. And after 48 h, the medium was then collected. The collected ADSC-CM was sterilized with 0.22 μm syringe filter (Millex-GS Syringe Filter Unit, MA, USA) after centrifugation at 300 × *g* for 5 min.

The collected ADSC-CM was diluted and divided into three groups: 100% ADSC-CM group, 50% ADSC-CM group, and 25% ADSC-CM group. The 100% ADSC-CM group (CM1) contained 10 mL collected ADSC-CM without any dilution. The 50% ADSC-CM (CM2) group contained 5 mL collected ADSC-CM and 5 mL DMEM. And the 25% ADSC-CM group (CM3) contained 2.5 mL collected ADSC-CM and 7.5 mL DMEM. All of these three groups of ADSC-CM were stored at −20 °C to maintain complete biological activity in the liquid state over extended periods [28]. After that, the freeze-drying process was conducted by a freeze dryer (Wuxi Voshin Instruments Manufacturing Co. LTD) according to the practical guidline.

2.4. Fabrication of electrospun fibrous scaffolds

Four types of electrospun fibers were investigated: micro-nano PLA fiber (MPF), the micro-nano PLA fiber containing CM1 lyophilized powder (MPF@CM1), the micro-nano PLA fiber containing CM2 lyophilized powder (MPF@CM2), the micro-nano PLA fiber containing CM3 lyophilized powder (MPF@CM3). In order to investigate the structure and biocompatibility of materials, we introduced PLA electrospun fiber (PF).

The electrospinning solution of PF was obtained by mixing and stirring 1 g PLA (Jinan Daigang Co. China), 6.42 mL dichloromethane (DCM) and 3 mL N, N-dimethylformamide (DMF) as previous described [29]. 1 mg HA (Yuancheng Technology Co. Wuhan, China) was respectively dissolved in 1 mL distilled water, 1 mL distilled water containing CM1 lyophilized powder derived from 10 mL CM1, 1 mL distilled water containing CM2 lyophilized powder derived from 10 mL CM2 and 1 mL distilled water containing CM3 lyophilized powder derived from 10 mL CM3 to make 1 wt% HA hydrosol. All of these mixtures were stirred until completely dissolved. Afterwards, a solvent mixture containing 6.42 mL DCM and 0.01 g Span-80 was respectively mixed with 200 μL the above mentioned HA hydrosol. The mixture was stirred at a high speed to obtain water-in-oil (W/O) emulsions containing uniformly micro-sol particles (Figure S1). At last, 1 g PLA and 3 mL DMF were dissolved in the emulsion to obtain electrospinning solutions for MPF, MPF@CM1, MPF@CM2, and MPF@CM3 fabrication.

The procedure of the electrospinning method was performed as described elsewhere [30]. Briefly, the electrospinning solutions were added to a 10 mL syringe equipped with a steel blunt needle with inner diameter of 0.9 mm and was electrospun at the flow rate of 80 μL/min controlled by a microinject pump (Lange Medical Instrument Co.,

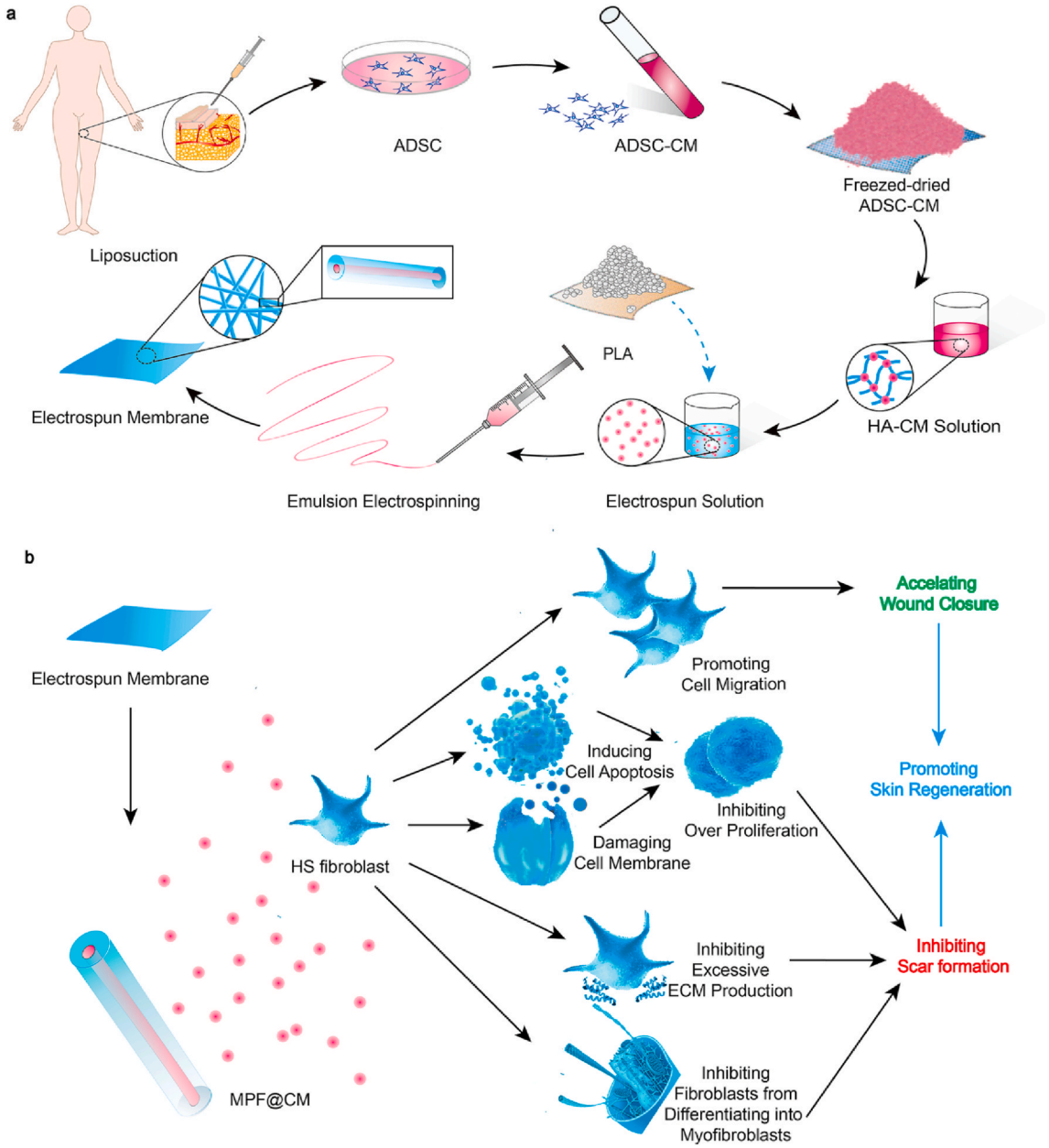

Fig. 1. Structure and function diagram of MPF loaded with ADSC-CM. (**a**) Preparation process of ADSC-CM loaded MPF. CM of ADSCs obtained by liposuction are freeze-dried and encapsulated inside HA nanoparticles, which constitutes the core of MPF@CM. (**b**) The pro-scarless skin regeneration effect of MPF@CM. ADSC-CM is released from the MPF@CM and acts on the surrounding fibroblasts to accelerate wound healing by promoting cell migration, and inhibits scar formation by limiting the over proliferation, inhibiting pathological differentiation of fibroblasts, and suppressing excessive ECM deposition.

Baoding, Hebei, China). The end of needle was attached with a metal clip which was connected to the DC high-voltage power supply (Tianjin Dongwen High-voltage Power Supply Co., China) set to 10–25 kV. At a distance of about 15 cm from the tip of the needle, an electrically grounded aluminum foil was used to collected electrospun fibers. All electrospun membranes were vacuum-dried overnight to completely remove any residual solvent before usage.

2.5. Characterization of electrospun fibers

2.5.1. Morphological characterization

In order to observe the microstructural morphology, samples of appropriate size were mounted on the scanning electron microscope (SEM) sample stub via conductive tapes. After sputter-coated with platinum (Quorum Technologies, SC7620, UK), the fibers were observed with a SEM (Hitachi, S-4800, Japan) at an accelerating voltage of 10 kV. The inner structure of individual fiber was verified by transmission electron microscopy (TEM, Hitachi, HT7700, Japan) at a voltage of 120 kV. And the average diameters of both the external structure and the inner structure were analyzed by measuring a total of 100 random fibers with Image J software (National Institutes of Health, Bethesda, MD).

2.5.2. Release assay

For release assay, 1 g fibrous membranes of both ADSC-CM loaded groups and MPF group were divided into two identical sections: one was used to measure the actual load of ADSC-CM by dissolved and extracted respectively by DCM and PBS; the other was immersed in 10 mL PBS and was placed in a thermostatic water bath at 37 °C for 7 days and 15 days respectively. With original ADSC-CM diluted to a 10%

concentration as reference, the extraction liquid and releasing buffer was collected and then measured by ultraviolet spectrophotometry. In addition, in order to investigate the release performance of loading cytokines and detect the corresponding concentration in its releasing buffer, we tested the most important cytokines during wound healing process, including bFGF, EGF, TGF-β1, VEGF, of the collected buffer by ELISA.

2.5.3. Biocompatibility evaluation of electrospun membrane

The electrospun membranes collected for cell direct contact culture were sterilized by electron-beam irradiation using linear accelerator (Precise™, Elekta, Crawley, UK) with a total dose of 80 cGy prior to the cell culture work. The biocompatibility of the membranes was determined by a direct method between electrospun membranes and HSFs. Briefly, HSFs were seeded at a density of 4×10^4 cells per well onto different membranes which were placed in 24-well culture plates. After 1 day and 3 days of culture, cells seeded were stained with a Live/dead Cell Double Staining Kit (Sigma-Aldrich, USA) for 30 min at room temperature and were examined under the Olympus IX71 light microscope (Olympus, Tokyo, Japan). Furthermore, the adhesive morphologies of HSFs on PF, MPF or MPF@CM electrospun membranes on day 3 were detected by phalloidin staining and examined with Confocal Laser Scanning Microscope (CLSM, Leica TCS SP2, Germany).

2.6. Evaluation of the biological effect of MPF@CM in vitro

2.6.1. Cell viability assay

The HSFs were incubated with releasing buffer which was collected on day 7 and sterilized by filtration at 37 °C with 95% relative humidity and 5% CO_2 partial pressure. The morphologies of HSFs were observed on day 1 and day 3. Compared with control, the effect of MPF@CM1, MPF@CM2, MPF@CM3, and MPF on cell growth and apoptosis was studied by a Cell Counting Kit-8 (Dojindo Molecular Technologies, Tokyo, Japan) and a Dead Cell Apoptosis Kit with Annexin V Alexa Fluor® 488 and propidium iodide (PI) for flow cytometry (Gibco, USA). In addition, a Cytotoxicity Detection Kit (Sigma-Aldrich, USA) was used according to the operation manual to detect the toxic effects of the biomaterials on cells.

2.6.2. Migration assay

HSFs were seeded at a density of 5×10^5 cells per well into 6-well culture plates. After cells attached firmly, the confluent monolayer of cells was scratched with a 200-μL pipette tip smoothly to induce a gap without cell attachment, and the cells were cultured for 24 h. Images were collected at the same positions of the plate at different time points post-scratching. Images were quantified using Image J software that measured the migrated area.

2.6.3. Wound regeneration-related protein expression detection by qRT-PCR and western blot

qRT-PCR and western blot was performed for protein expression detection as previously reported [31]. Briefly, total HSF RNA were extracted after 24 h of incubation with releasing buffer of different groups by using a RNA isolation kit (Takara Bio, Shiga, Japan). RNA purity was evaluated by calculating the A260/A280 ratio, aiming for a value of 1.8–2.1. The primer pairs (human) used for gene amplification from the cDNA template were as follows: Col I: forward 5′- GAGGGC AACAGCAGGTTCACTTA-3′ and reverse 5′-TCAGCACCACCGATGT CCA-3′; Col III: forward 5′- CCACGGAAACACTGGTGGAC-3′ and reverse 5′- GCCAGCTGCACATCAAGGAC-3′; α-SMA: forward 5′-GACAATGGC TCTGGGCTCTGTAA-3′ and reverse 5′-TGTGCTTCGTCACCCACGTA-3′; and glyceraldehyde 3-phosphate dehydrogenase (GAPDH): forward 5′-GCACCGTCAAGCTGAGAAC-3′ and reverse 5′-TGGTGAAGACGCCAGT GGA-3′. The results from three independent reactions were normalized against the expression level of the GAPDH control and used to determine the relative expression levels of the target genes.

After 24 h of culture, total protein was extracted with RIPA lysis buffer as described previously [31]. The protein was incubated with antibodies of Col I (Rabbit, 1:3000; Abcam, Cambridge, UK), Col III (Rabbit, 1:1000; Abcam, Cambridge, UK), α-SMA (Rabbit, 1:1000; Abcam, Cambridge, UK) and β-actin antibodies (Goat, 1:500; Santa Cruz Biotechnology, Inc., Dallas, TX, USA). The immunoreactive traces were detected by using an enhanced chemiluminescence (ECL) detection kit (Amersham Biosciences, Chalfont St. Giles, UK). The intensity of protein expression on the membranes was analyzed by Image J software.

2.7. Evaluation of the biological effect of MPF@CM in vivo

2.7.1. Preparation for in vivo study

Male C57BL/6 mice were purchased from the Experimental Animal Center of Shanghai Ninth People's Hospital (Shanghai, China). All surgical procedures as well as perioperative handling were conducted in accordance with protocols approved by the Ethics Committee at the Shanghai Ninth People's Hospital.

For the *in vivo* animal experiment, mouse ADSCs (mADSCs) were isolated from the subcutaneous adipose tissue in groin of C57BL/6 mouse [32]. The methods for conditioned medium of mADSCs (mADSC-CM) collection and the fabrication for mADSC-CM loaded electrospun membranes is the same as that we described in the section of experiments *in vitro*.

The *in vivo* wound healing experiments were carried out by a full thickness skin defect model as described previously [31]. Briefly, C57BL/6 mice (20–25 g, 8-10-week age) with a full-thickness excisional wounds of 1.5 cm × 1.5 cm were randomly divided into five groups (n = 3). Wounds were covered with MPF@CM1, MPF@CM2, MPF@CM3, or MPF electrospun membranes for 15 days.

2.7.2. Wound healing obervation

Wounds were photographed with a digital camera every 3 days. To evaluate the size of the wound and the scar formation, the area of the wound was measured by Image J software as described previously [33].

2.7.3. Histologic analysis

H&E, Masson's trichrome, and immunohistochemistry staining were conducted to observe the microscopical features of wound healing as described previously [31]. The wound healing samples *in vivo* collected on day 15 were embedded in paraffin blocks and cut into 4-μm thick tissue sections at the midline of the obtained tissue. Routine H&E staining and Masson's trichrome staining were performed for the micro morphology observation and collagen fibers analysis. For immunohistochemistry staining, antibodies against Col I (1:100; Abcam, Cambridge, UK), Col III (1:100; Abcam, Cambridge, UK), MMP1 (1:100; Abcam, Cambridge, UK), TIMP1 (1:100; Abcam, Cambridge, UK), and α-SMA (1:100; Abcam, Cambridge, UK) were used to access the ECM deposition and HS formation. VEGF (1:100; Abcam, Cambridge, UK) and epidermal thickness revealed in H&E staining were indexes of angiogenesis and epidermal proliferation [34,35]. Images were photographed under bright field microscope (Olympus, Tokyo, Japan). The degree of positive staining during immunohistochemical labeling depends on the antigen content, distribution density, labeling method and sensitivity. The main methods for histological immunohistochemical analysis is staining intensity scoring method, which scores the protein expression according to the staining intensity and the staining positive range. The optical density value is directly related to the staining intensity of the dyed tissue. Image J automatically scores tissue protein expression by calculating the optical density value, avoiding the deviation caused by human counting or evaluation [36,37]. Thus, Image J software was used for statistical analysis of area positive-stained here. And the statistical differences which were determined by One-way ANOVA followed by Tukey's multiple comparison test were evaluated by SPSS.

In order to further verify the expression of the above proteins in tissues, we also carried out qRT-PCR detection on tissue samples collected on day 15. Here we detected the transcription level of proteins that best reflects the characteristics of pathological scars, and explored the key regulatory proteins in the process of wound healing and scar formation, including Col I, Col III, MMP1, TIMP1, α-SMA, and VEGF. The primer pairs (mouse) used for gene amplification from the cDNA template were as follows: Col I: forward 5′-TGACTGGAAGAGCGGAGAGTA-3′ and reverse 5′-GACGGCTGAGTAGGGAACAC-3′; Col III: forward 5′-TCTTATTTTGGCACAGCAGTC-3′ and reverse 5′-GTGGCTCCTCATCACAGATTA-3′; MMP1: forward 5′-ATGATGATGATGACCTGTCTG-3′ and reverse 5′-CACCTCTAAGCCAAAGAAAGAT-3′; TIMP1: forward 5′-CCAGAACCGCAGTGAAGAGT-3′ and reverse 5′-GTACGCCAGGGAACCAAGA-3'; VEGF: forward 5′-CTCACTTCCAGAAACACGA-3′ and reverse 5′-GGGTGCTTTTGTAGACTATCA-3′; α-SMA: forward 5′-CCTGAAGAGCATCCGACACT-3′ and reverse 5′-CACAGCCTGAATAGCCACATAC-3′; and GAPDH: forward 5′-CCTCTATGCCAACACAGT-3′ and reverse 5′-AGCCACCAATCCACACAG-3′. The results from three independent reactions were normalized against the expression level of the GAPDH control and used to determine the relative expression levels of the target genes.

2.8. Statistical analysis

Data are representative of three or more independent experiments. Statistical differences (*$p < 0.05$) were determined by One-way ANOVA followed by Tukey's multiple comparison test. Results were expressed as mean ± standard deviation (SD).

3. Results

3.1. MPF@CM effectively release encapsulated ADSC-CM

ADSCs can be conveniently obtained from adipose tissue by enzymatic digestion, showing a homogeneous surface immunophenotype and processing the potential to differentiate into adipocytes, osteoblasts, and other cells, both *in vivo* and *in vitro* [38]. After three passages *in vitro*, ADSCs exhibited an elongated fibroblast-like morphology (Figure S2a). They differentiated into osteoblastic and adipocytic lineages (Figure S2b, c), showing their pluripotency. In these cells, flow cytometry revealed that the hematopoietic markers, including CD31, CD34, and CD45, were negative, however, the expressions of CD29, CD90 and CD105 were positive, like other mesenchymal stem cells (Figure S2d).

After diluting and freeze-drying CM from cultured ADSC, the lyophilized powder was encapsulated into micro-nano fibrous scaffolds. According to the preparation process and CM concentration delivered, there are five groups: PF group, MPF@CM1 group, MPF@CM2 group, MPF@CM3 group, and MPF group as described in the method section. Fig. 2e showed a 1 wt% HA hydrosol containing either CM1, CM2, or CM3 lyophilized powder, the color of which varied with the concentration. These groups were characterized by morphological observation and release study.

The surface morphology of these membranes was shown in Fig. 2a, where the fibers were uniform, smooth and randomly oriented. Membrane pores vary in diameter from a few nanometers to a few microns, which facilitates the exchange of nutrients and waste, while providing a barrier to external pathogens and preventing excessive bleeding [39]. TEM observation showed that the core-shell structure of MPF fiber with HA as the center was different from that of PF fiber with no core (Fig. 2b). With the protection of HA, the integrity and bioactivity of cytokines secreted by ADSCs can be maintained, and the initial burst of fibers could be alleviated, thus to improve the performance of scaffold [33]. The average core diameters of MPF@CM1, MPF@CM2, MPF@CM3, and MPF were 0.657 ± 0.2 μm, 0.579 ± 0.197 μm, 0.559 ± 0.196 μm, and 0.413 ± 0.18 μm, respectively. The average shell diameters of PF, MPF@CM1, MPF@CM2, MPF@CM3, and MPF were 1.09 ± 0.287 μm, 1.206 ± 0.343 μm, 1.201 ± 0.351 μm, 1.147 ± 0.34 μm, and 1.153 ± 0.332 μm, respectively. The addition of CM lyophilized powder slightly increased the core diameter, which also increased the overall diameter of fibers (Fig. 2c).

To evaluate the local sustained release effect of CM loaded electrospinning membranes, the releasing buffer of MPF@CM1, MPF@CM2, MPF@CM3, and MPF collected on day 7 was measured by ultraviolet spectrophotometry. The releasing buffer showed a characteristic waveform as original ADSC-CM diluent with double peaks at 430 and 560 nm (Fig. 2d). The release rates for 7 days of MPF@CM1, MPF@CM2, and MPF@CM3 were 51.53%, 39.51%, and 24.35%, respectively (Fig. 2f). Similarly, the release rates for 15 days of MPF@CM1, MPF@CM2, and MPF@CM3 were 84.33%, 73.67%, and 38.67%, respectively (Figure S3). The release rate of the fibers with high CM was higher than that of the fibers with low CM concentration, indicating the controllability of the release behavior. The release performance of the detected four critical cytokines (bFGF, EGF, TGF-β1, VEGF) is the same as the overall release trend detected by ultraviolet spectrometer (Figure S4). The culture medium was successfully loaded in the electrospun fibers, and the effective concentration of cytokines can be detected in releasing buffer of 7 days and 15 days.

3.2. MPF@CM shows high biocompatibility

Biocompatibility is an essential character for biomaterials, which can be used to predict whether a material will cause potential danger for patients [34,40]. Here, the membranes were implanted with HSFs to evaluate their biocompatibility. After 3 days of culture, the cells were spindle shaped, and there was no significant difference in the morphology of cells growing on different membranes (Fig. 3a). Live-dead staining kit was used to indicate survival condition of HSFs on day 1 and day 3. Growing on the membrane surface, the living cells were green and the dead cells were red (Fig. 3b and c). On day 3, compared with day 1 (Fig. 3d and e), the proportion of living cells inoculated on the membrane decreased slightly, which might be attributed to the hydrophobicity of the membrane.

3.3. Evaluation of the biological effect of MPF@CM in vitro

The molecular mechanism of HS is associated with the abnormal over proliferation and transition of fibroblasts and the excessive production of ECM, including Col I and Col III [38]. During wound repair, fibroblasts are activated and differentiate into myofibroblasts characterized by α-smooth muscle actin (α-SMA). Myofibroblasts migrate to the defect and secrete massive ECM components, playing a central role in scar formation [41,42]. Thus, inhibition of the overproliferation and ECM production of myofibroblasts is a pivotal measure against fibrosis and abnormal scar formation.

Due to the tendency of HSFs to abnormally differentiate into myofibroblast, produce excessive ECM, and uncontrolled overproliferate, HSF is a good experimental cell to investigate the effect of MPF@CM on promoting normal skin regeneration. Here, releasing buffer of different electrospinning membranes was collected to conduct the *in vitro* experiment. Although there is no difference of the morphology of all the groups on day 1 and day 3, the cell density seems to decrease in MPF@CM groups after 3 days of culture (Fig. 4a). To further investigate the cellular mechanism of MPF@CM, we performed a CCK8 assay, flow cytometric analysis, and a cytotoxicity assay, to detect the proliferation and apoptosis of HSFs, and the cell membrane damaging effect of electrospun membranes.

For CCK8 analysis, there was no significant difference in OD value in the first 36 h. But with the passage of time, the proliferation difference between the two groups was significant. MPF@CM1 showed an obvious effect of inhibiting cell proliferation. MPF@CM3 didn't show an inhibiting effect compared with the control group and MPF (Fig. 4c).

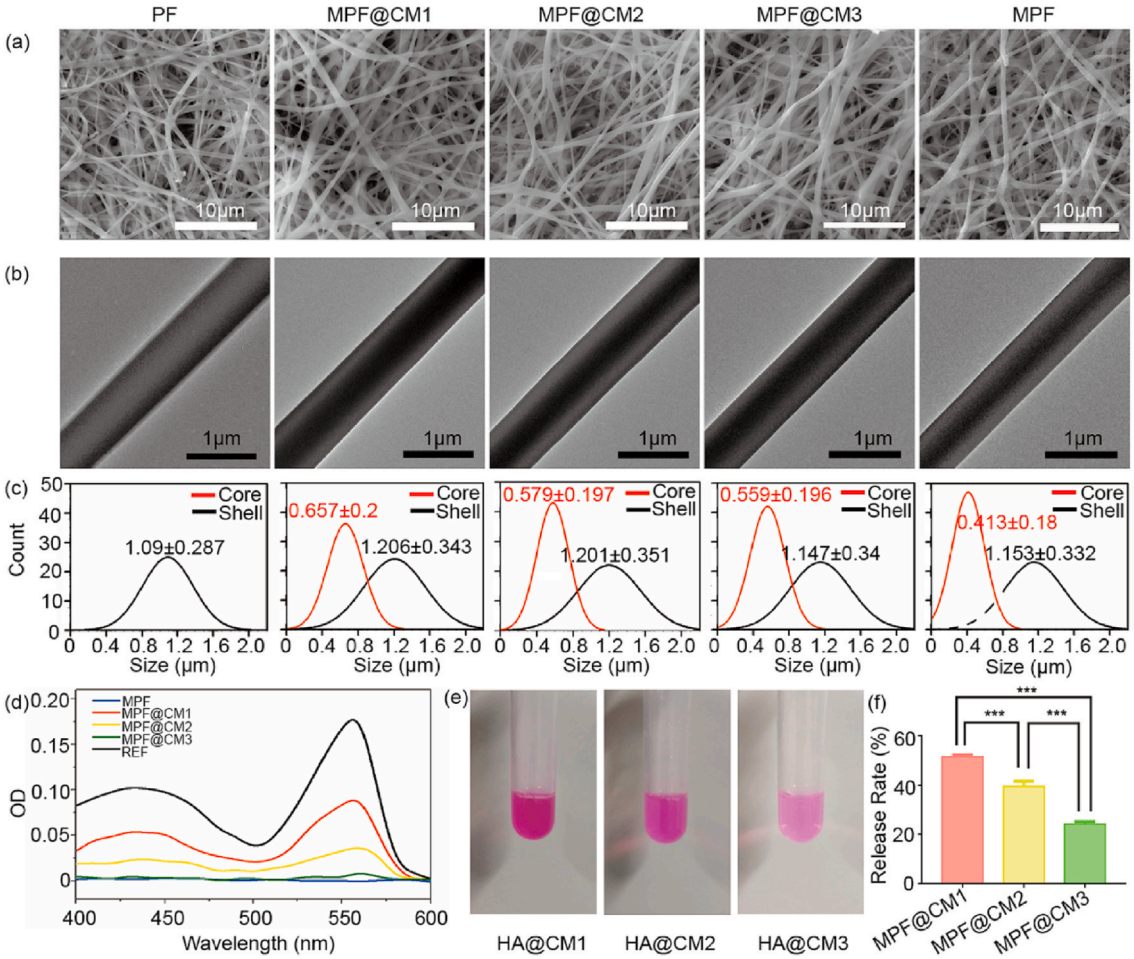

Fig. 2. ADSC-CM loaded by MPF @ CM effectively release *in vitro*. (**a**) Surface morphology of membrane composed of MPF@CM. (**b**) The core-shell structure of MPF@CM observed by TEM. (**c**) Core and shell diameters of fibers (Average ± SD, n = 100 for each group). (**d**) Ultraviolet spectrophotometry of releasing buffer of fibers collected on day 7 and (**f**) the release rate of MPF@CM for 7 days (Average ± SD, n = 6 for each group, *** denotes $P < 0.001$ by One-way ANOVA followed by Tukey's multiple comparison test). (**e**) The shades of color with the changes of concentration of ADSC-CM encapsulated in HA nanoparticles.

This may be due to the fact that MPF@CM with a low concentration of CM has a smaller total load and slower release rate, as we observed in the release study. Flow cytometry image analysis (Fig. 4b) showed the total apoptosis rate of MPF @ CM1 group was slightly higher than that of the control group, MPF @ CM3 group, and MPF group, which was statistically significant (Fig. 4d).

Unexpectedly, the releasing buffer of MPF@CM1 showed a notable effect on destroying fibroblast membrane, and the damage rate was close to 25%. With the decrease of ADSC-CM concentration, the cell injury rate decreased (Fig. 4e). Without knowing the exact bioeffectors, the components of ADSC-CM and their potential biological mechanisms need to be further investigated.

An *in vitro* scratch assay was performed to evaluate the migration ability of fibroblasts which largely determines the wound healing rate [43]. As cells on both sides of the gap caused by scratch migrated to the center gradually, the distance between cells became shorter. After 24 h of culture, compared with the control group and MPF group, the distance between two sides of the gaps in MPF@CM1 group, MPF@CM2 group, and MPF@CM3 group were much shorter (Fig. 5a). To quantify the differences between the groups, we compared the relative scratch areas of 0-h, 6-h, 12-h, and 24-h. As shown in Fig. 5c, the pro-migration effect of MPF @ CM1 was first observed after 6 h of culture. At 24-h, the relative scratch area of MPF@CM groups was much smaller than that of the control group and MPF group. With the increase of ADSC-CM load concentration, the difference was more obvious, which showed that MPF@CM had the promoting effect on fibroblast migration.

HSFs were stimulated with the releasing buffer of MPF@CM1, MPF@CM2, MPF@CM3, and MPF for 24 h. MPF@CM decreased the expression of Col I, Col III, and α-SMA in a concentration-dependent manner at mRNA and protein levels (Fig. 5b, d-f). The relative quantity of Col I and Col III, and the percentage of α-SMA-positive HSFs were significantly lower in the MPF@CM1 group. There was no difference between the control group and MPF group, suggesting that the degradation products of PLA and HA has no effect on ECM production and fibroblast differentiation.

Taken together, these data showed that the degradation products of MPF had no significant effect on the activity of HSFs. However, from the perspective of apoptosis induction, cell membrane damage, fibroblast differentiation inhibition, and ECM production suppression effects of MPF@CM, the delivered ADSC-CM possessed a tremendous potential for inhibiting abnormal scar formation.

3.4. MPF@CM effectively promotes skin regeneration in vivo

Based on the above-mentioned promoting regeneration effect of MPF@CM *in vitro*, a mouse dorsal full-thickness skin defect model was established for *in vivo* evaluation. In brief, once the wound was formed, it was covered with an electrospun membrane, and assessment of wound area with images was performed every three days (Fig. 6a). After 6 days of treatment, the wound areas of MPF@CM1 group were much smaller than that of the control group, MPF group, and MPF@CM3 group. The differences were clearer with time elapsed. On

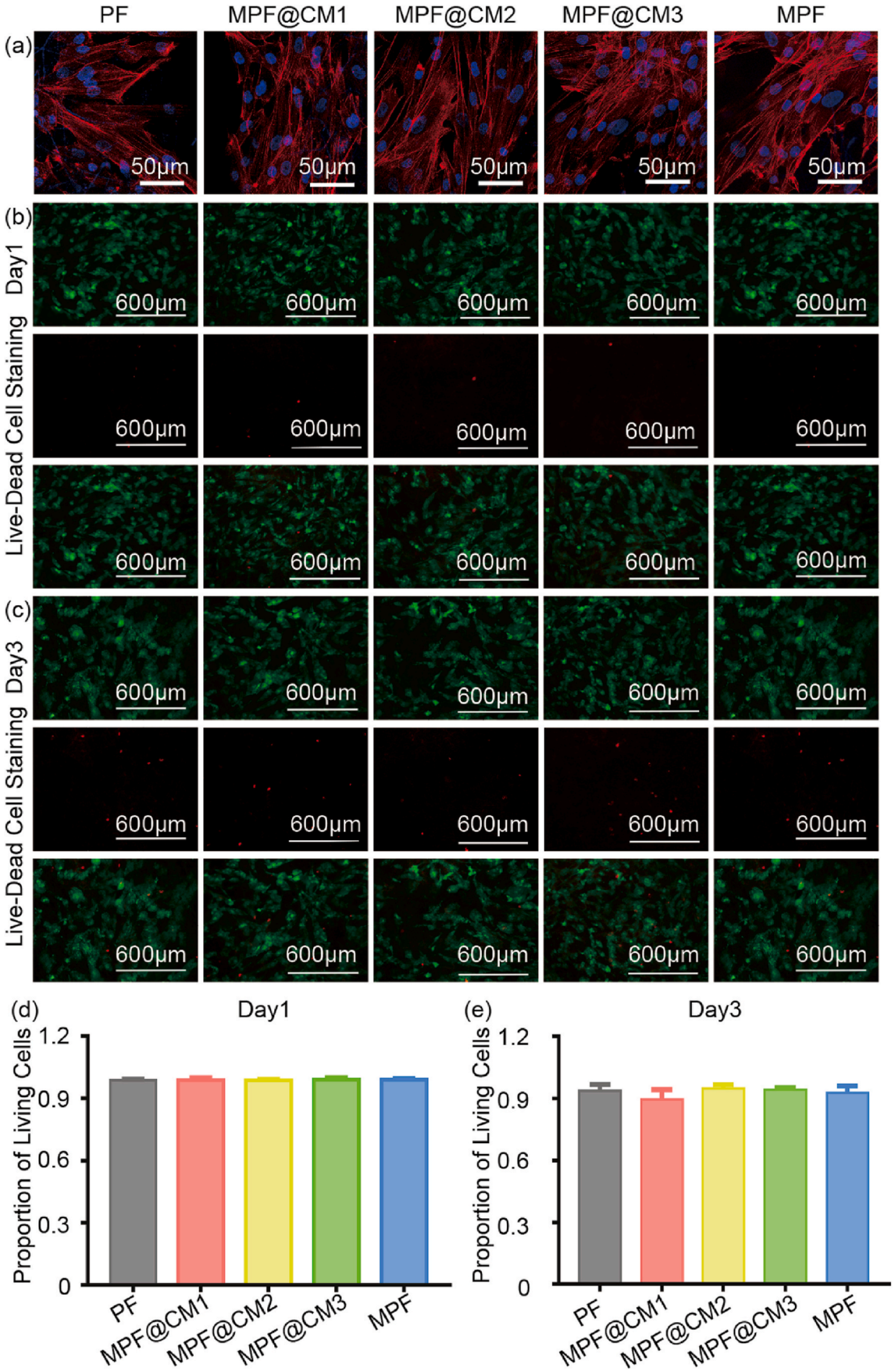

Fig. 3. Morphology and survival rate of fibroblasts seeded on electrospun membranes. (**a**) Morphology of fibroblasts with cytoskeleton staining seeded on electrospun membranes for 3 days. Fibroblasts seeded on electrospun membranes for (**b**) 1 day and (**c**) 3 days are stained with live-dead staining kits that make live cells green and dead cells red. The survival rate of fibroblasts cultured for (**d**) 1 day and (**e**) 3 days on electrospun membranes (Average ± SD, n = 6 for each group).

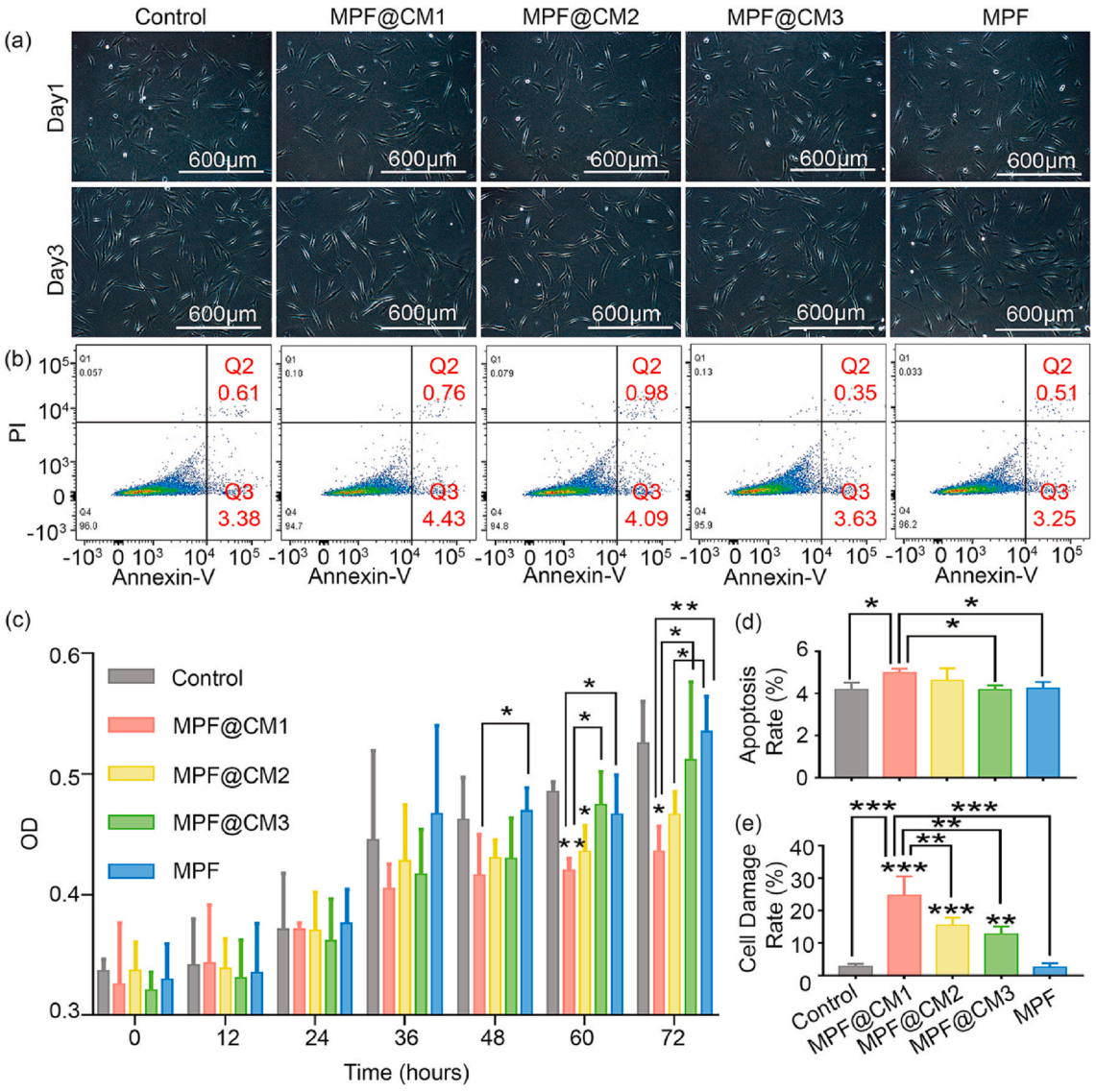

Fig. 4. MPF@CM significantly inhibits fibroblast proliferation. (**a**) Morphology of fibroblasts cultured for 1 day and 3 days. (**b**) The flow cytometry and (**d**) analysis of apoptosis rate (Average ± SD, n = 3 for each group, * denotes P < 0.05 by One-way ANOVA followed by Tukey's multiple comparison test). (**c**) CCK8 cell proliferation assay (Average ± SD, n = 3 for each group, * denotes P < 0.05 and ** denotes P < 0.01 by One-way ANOVA followed by Tukey's multiple comparison test). (**e**) LDH cytotoxicity detection. (Average ± SD, n = 3 for each group, ** denotes P < 0.01 and *** denotes P < 0.001 by One-way ANOVA followed by Tukey's multiple comparison test).

day 12, the wound area of MPF@CM1 group was only 34.9% of that of the control group, indicating the significant effect of MPF@CM on accelerating wound closure. Wounds of all groups were almost closed after 15 days (Fig. 6b). Surprisingly, after closure of wounds, the scars of MPF@CM1 group and MPF@CM2 group were barely noticeable, indicating that MPF@CM had significant effect on promoting normal skin regeneration, inhibiting fibrosis, and quickly restoring the appearance and function of damaged skin *in vivo* (Fig. 6c). In addition, during the observation period, there was no redness, swelling, ulceration or poor wound healing in the part where the biomaterial was applied and mice did not show obvious poor appetite or weight loss, showing the safety of MPF@CM in-vivo application.

To further investigate the expression of scar-related proteins in tissue and verify the anti-fibrosis effect of MPF@CM histologically, Masson's trichrome staining and immunohistochemistry staining were performed (Fig. 7a–h). MPF@CM significantly inhibited ECM deposition, including Col I and Col III (Fig. 7j-l). In the MPF@CM groups, collagen in the dermis was thin and orderly arranged (Fig. 7b). There was no significant difference in the expression of TIMP1, a key factor to inhibit ECM degradation (Fig. 7n). The lower expression level of MMP1, a protease promoting ECM degradation, in MPF@CM1 group and MPF@CM2 group (Fig. 7m) may be a regulatory response to low ECM deposition [44]. In addition, the decreased expression of α-SMA in MPF@CM (Fig. 7p) showed an inhibitory effect on fibroblast differentiation, which was consistent with the result of the *in vitro* experiment. Vascular endothelial growth factor (VEGF) is an essential factor for vascular formation, which can increase the survival, proliferation and migration of vascular endothelial cells. New blood vessels are essential for tissue repair because they support cells in the wound with nutrition and oxygen [45]. Although the inhibition of VEGF activity with the injection of anti-VEGF antibodies has been shown to reduce scar formation [46], this treatment strategy can cause ischemic injuries and inhibit wound regeneration. In our study, groups with less collagen deposition and smaller scar area showed more VEGF expression and a faster healing rate (Fig. 7o), indicating that MPF@CM promoted scar-free wound healing by simultaneously inducing angiogenesis. The changes of the above proteins, including col I, col III, TIMP1, MMP1, VEGF, and α-SMA have been further verified at the RNA expression

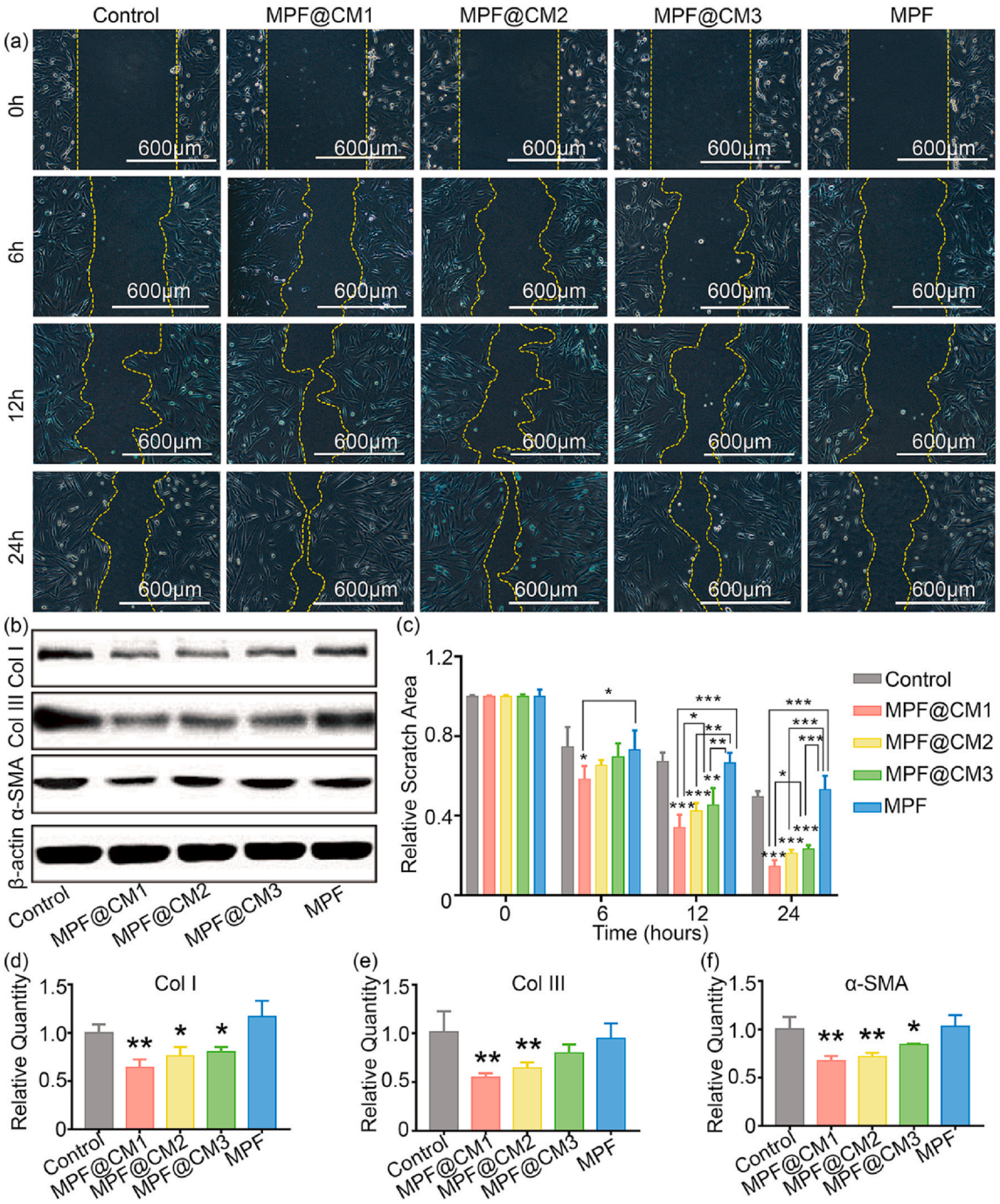

Fig. 5. MPF@CM promotes the migration of fibroblasts and inhibits the expression of scar-related protein. (**a**) Morphological and (**c**) quantitative analysis of HS fibroblasts migration area on 0-h, 6-h, 12-h, and 24-h (Average ± SD, n = 6 for each group, * denotes P < 0.05, ** denotes P < 0.01 and ***denotes P < 0.001 by One-way ANOVA followed by Tukey's multiple comparison test). (**b**) Western blot analysis of Col I, Col III, and α-SMA. Quantitative real-time PCR analysis of (**d**) Col I, (**e**) Col III, and (**f**) α-SMA. (Average ± SD, n = 3 for each group, * denotes P < 0.05, ** denotes P < 0.01 and *** denotes P < 0.001 by One-way ANOVA followed by Tukey's multiple comparison test).

level of the collected tissue, which was in accordance with the above immunohistochemistry staining results (Figure S5).

The change of epidermal thickness is the direct indicator of epidermis hyperplasia or differentiation [47]. In order to investigate the effect of MPF@CM on the epidermis, we compared the epidermal thickness of five groups, and there seemed to be no differences between the five groups (Fig. 7i).

Thus, the *in vivo* experiment demonstrated that MPF@CM was an effective cell-based biomaterial to accelerate wound healing and prevent abnormal scar formation, which can promote angiogenesis without adversely affecting epidermal cells.

4. Discussion

In this study, an ADSC-CM loaded electrospun fiber (MPF@CM) was constructed through protein freeze-drying technology and emulsion electrospinning technology. The material characterization showed that the electrospinning has a unique core-shell structure, which not only protected the biological activities of various substances encapsulated in the core, but also showed a long-term controlled release effect. *In vitro*

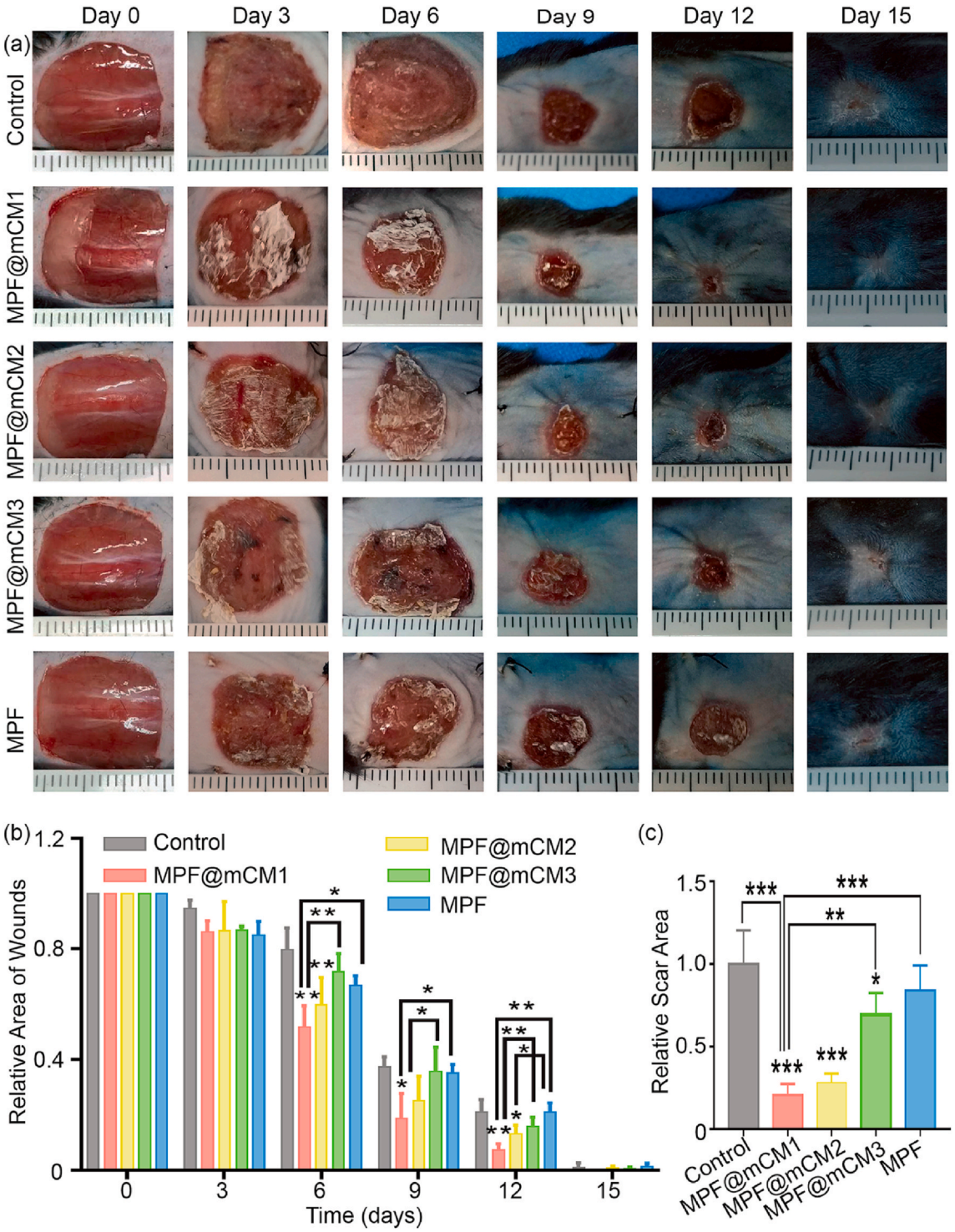

Fig. 6. MPF@CM promotes wound healing and inhibits scar formation *in vivo*. (**a**) Compared with the control and MPF, MPF@CM promotes skin regeneration *in vivo*. Statistical analysis of the healing of (**b**) skin defect and (**c**) scar area (Average ± SD, n = 3 for each group, * denotes P < 0.05, ** denotes P < 0.01 and *** denotes P < 0.001 by One-way ANOVA followed by Tukey's multiple comparison test).

and *in vivo* experiments showed that the biologically active substances released MPF@CM directly acted on fibroblasts, significantly promoting skin regeneration. Thus, based on pro-regenerative effect of ADSC-CM, this study proposed a practical biomaterial mediated cell-free regeneration strategy.

ADSC is a multipotent MSC which is readily accessible by liposuction, easier to isolate and carry a significantly lower morbidity [48]. ADSCs have displayed regenerative capacity when applied to a range of human disease [49,50]. Currently, it is believed that the regenerative therapeutic effect *in vivo* of ADSCs is achieved mainly through releasing bioactive substances by a paracrine manner, including cytokines, growth factors, signaling lipids, and nucleic acids [51–54]. They resemble the effect of parental stem cells, modulate the activity of recipient cells, and play important roles in promoting tissue regeneration [16,55]. Compared with ADSCs, ADSC-CM that contains cell-secreted products but without cellular components demonstrated several

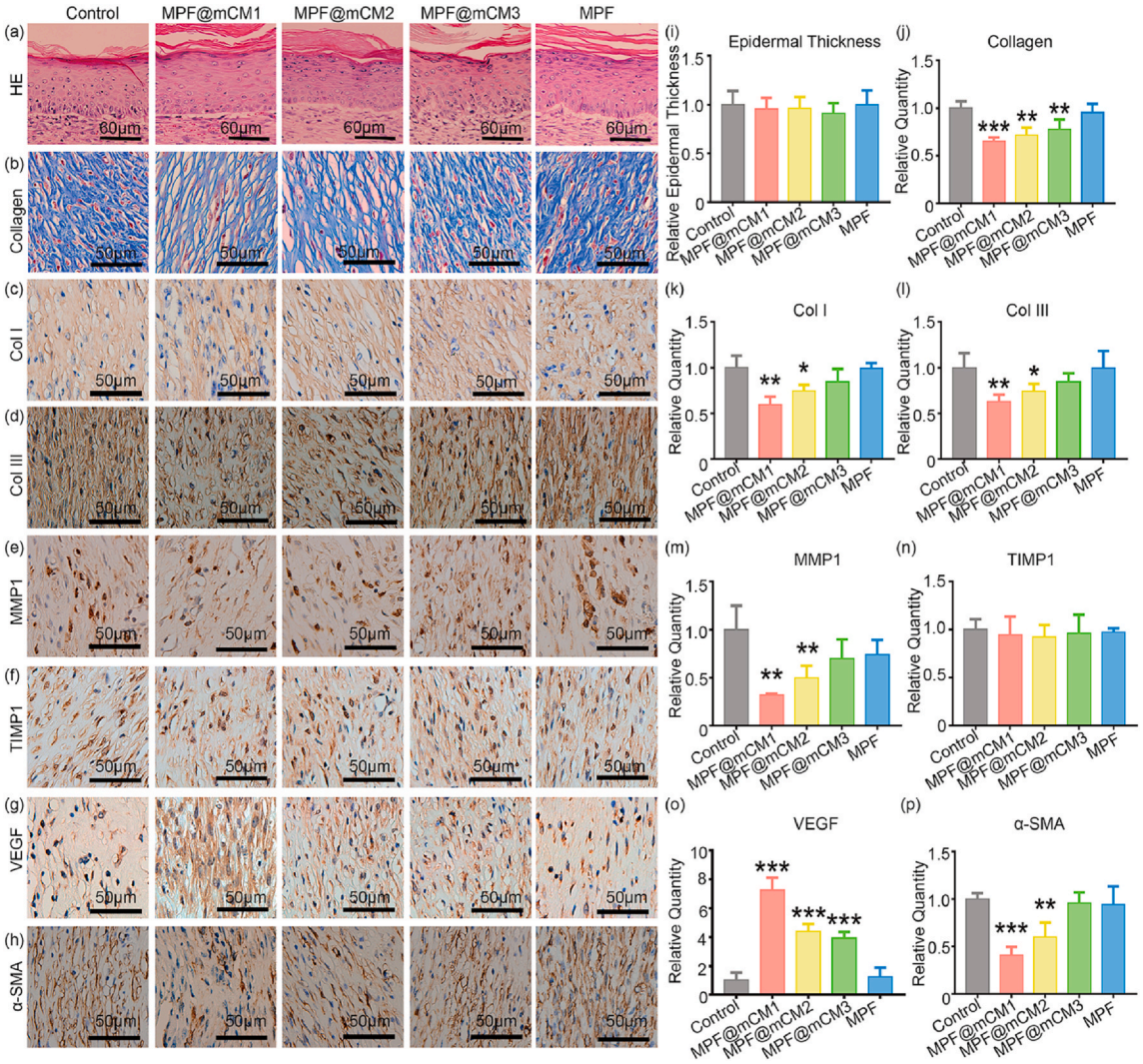

Fig. 7. Histological analysis of scar tissues. (**a**) HE staining of epidermal layer and (**b**) Masson staining of dermal collagen deposition. Immunohistochemical staining of (**c**) Col I, (**d**) Col III, (**e**) MMP1, (**f**) TIMP1, (**g**) VEGF, and (**h**) α-SMA. Statistical analysis of (**i**) epidermal thickness, (**j**) dermal collagen deposition, and the expression of (**k**) Col I, (**l**) Col III, (**m**) MMP1, (**n**) TIMP1, (**o**) VEGF, and (**p**) α-SMA. (Average ± SD, n = 3 for each group, * denotes $P < 0.05$, ** denotes $P < 0.01$ and *** denotes $P < 0.001$ by One-way ANOVA followed by Tukey's multiple comparison test).

therapeutic benefits for regenerative treatment application: (1) Applicability of allogeneic therapy: Because of different major histocompatibility complexes (MHC) antigen on cell membrane expressed by derived from different individuals, allogeneic cell grafting therapy result in uncontrolled immune responses and tissue destruction and can lead to inflammatory disorders [56,57]. While MSC-CM contains no cell membrane epitope, the deliverance of which effectively avoiding immune rejection and can be used for allogeneic therapy, expanding the scope of clinical applications. While MSC-CM contains no cell membrane epitope, the deliverance of which effectively avoiding immune rejection and can be used for allogeneic therapy, expanding the scope of clinical applications. (2) Controllable efficacy: Due to a series of treatment process before and during transplantation and the changes of microenvironment, the viability of the cells decreased. Translation of cells is hampered by challenges in maintaining optimal cell vitality, which are currently uncontrollable. In addition, as for the multi-directional differentiation potential of stem cells, there are still no effective measures to prevent local stem cell differentiation *in vivo* [11]. While the efficacy of MSC-CM can be precisely modulated by adjusting the local concentration and total dose delivered. (3) Safe for human body: studies have shown that MSCs can be serve as a direct cellular origin of cancer, which is closely related to the self-renewal capacity of stem cells [12]. Thus, cell free therapy proposed here is relatively safe to human body. (4) Convenient to store and transport: as conducted in this study, ADSC-CM can be stored with biological activities maintained for a long period after protein lyophilization technology treatment, which facilitates mass production and transportation of the biologically active substances. (5) Tremendous designed therapeutic potential: substantial evidence suggests that the biological characteristics of MSC-CM can be regulated by changing the preparation conditions, including oxygen tension, growth factor composition and mechanical properties [31,58]. Consequently, MSC-CM with specific therapeutic effect can be acquired in a designed way so as to promote regeneration in a targeted manner. Therefore, ADSC-CM is suggested as a novel cell-free medicinal product that can recapitulate the beneficial effects of ADSC and has various advantages in overcoming the limitations and risks associated with cell-based therapy.

However, despite the clear benefits of using MSC-CM for regenerative medicine reported, there are still several issues to be addressed for clinical practice. Due to the long duration of the healing process, the complexity of the components of MSC secreted substances, the structural and functional instability of biologically active substances, and the unpredictable biological distribution of direct drug application, the most important challenge is a lack of common

recommendations or standards for bioprocessing and clinical application of MSC-CM based therapeutics [59]. In this study, we suggested a biomaterial-based strategy that help to overcome these issues and, finally, optimize the development of MSC-CM based products in general. Here, ADSC-CM loaded micro-nano electrospun fiber (MPF@CM) was constructed by protein freeze-drying technique and emulsion electrospinning technology. Freeze-drying is a popular method to prepare pharmaceutical formulations containing structurally complex active ingredients [60]. In this study, the solidification performed at −20 °C significantly improves storage stability of the biological substances from ADSC-CM, which are marginally stable in aqueous solutions. After that, the freeze-dried powder was wrapped with HA nanoparticles, which further protect the unstable structure of biological substances from the additional damage caused by the violent emulsification process (i.e., high speed stirring, ultrasonication, or homogenization of the protein/polymer mixture prior to electrospinning) [61,62]. Due to the weakening effect of HA nanoparticles on the initial burst performance of drug-loaded fiber [29], the constructed fiber with core-shell structure showed a long-term controllable release performance, and the release rate decreases as the load of substances decreases. As the experimental results showed, MPF@CM1 with the largest CM load could release 51.53% of the total bioactive substances after 7 days; while in contrast, MPF@CM1 with the largest CM load only released 24.35% of the total bioactive substances loaded. Futhermore, from SEM, the relatively large surface area of electrospun fibers enables the full effect of bioactive substances released on local cells, and the porous structure of the scaffold guarantees the exchange of gases, water and nutrients, which is conducive to the regenerative repair of damaged tissue. Thus, in terms of the predominant biomaterial performance and the pro-regeneration effect of MSC-CM, the CM loaded fiber designed in this study is simple to prepare, easy to produce and store, safe and effective to use, showing great potential for clinical application.

Further, the therapeutic effect of MPF@CM was verified both *in vitro* and *in vivo*. For mammals, good wound healing not only requires a rapid healing speed to rapidly restore the local skin barrier, but also needs to return to normal appearances and functions. Due to the limited regeneration capacity of human beings, skin repair usually displays an unspecific form of healing in which the wound heals by fibrosis and scar formation [63,64]. HS formation is a common adverse result of wound healing, with an incidence of up to 77% after burns [65]. This incomplete regeneration results in cosmetic annoyance and functional impairment, including weird skin texture, limited local joint movement, and abnormal body temperature regulation, causing severe physical and psychological torture to the patients [66]. In order to more specifically observe the effect of MPF@CM on skin regeneration, we selected HSFs which were derived from HS tissue as the experimental cell *in vitro*. HSFs are characterized by producing large amounts of ECM and have a tendency to overproliferate, which are the responsible cells for tissue fibrosis and scar formation [67]. In *in vitro* experiments, the bioactive substances released by MPF@CM not only significantly promoted the migration of fibroblasts, but also inhibited the excessive proliferation of scar fibroblasts and abnormal deposition of ECM. In animal experiments, we observed a consistent conclusion: MPF@CM significantly accelerated wound closure, and promoted scar-free regeneration by inhibiting the excessive deposition of collagen I and collagen III, quickly restoring the normal appearance of skin. In addition, the experiments also proven the good biocompatibility of the biomaterial constructed, which supported cell adhesion and growth and caused no adverse reactions *in vivo*. This study only used a skin defect model to detect the regenerative effect of MPF@CM. However, because of the significant regulating effect of MPF@CM on fibroblast migration, ECM deposition, and blood vessel formation, it can also be served as tissue repair material for other damaged tissue repair. The morphological plasticity, biological safety, and therapeutic efficacy of MPF@CM make it useful for repairing various tissue defects and have tremendous clinical application prospects.

5. Conclusion

Based on the biological regulation function of bioactive substances derived from cells, we proposed CM-biomaterials for injured tissue regeneration. A controllable sustained release system loaded with CM was built up by protein freeze-drying and emulsion electrospinning technologies. In this study, the *in vivo* and *in vitro* experimental results suggested that the electrospun fibers loaded with ADSC-CM had significant promoting effect on skin regeneration. This study opened up a new way for the application of CM in the field of regenerative medicine, promoted the development of cell-based biomaterials, and provided theoretical and experimental basis for the further development and application of CM-biomaterial in regenerative therapy.

CRediT authorship contribution statement

Lu Chen: Methodology, Investigation, Writing - original draft. **Liying Cheng:** Validation, Formal analysis, Funding acquisition. **Zhen Wang:** Resources. **Jianming Zhang:** Writing - review & editing. **Xiyuan Mao:** Data curation. **Zhimo Liu:** Visualization. **Yuguang Zhang:** Supervision, Funding acquisition. **Wenguo Cui:** Conceptualization. **Xiaoming Sun:** Conceptualization, Project administration, Funding acquisition.

Declaration of competing interest

The authors declare that they have no conflicts of interests.

Acknowledgments

This work was supported by the National Natural Science Foundation of China (81701907, 81772099 and 81801928), Shanghai Sailing Program (18YF1412400), Pujiang program of SSTC (18PJ1407100).

Appendix A. Supplementary data

Supplementary data related to this article can be found at https://doi.org/10.1016/j.bioactmat.2020.08.022.

References

[1] P. Liu, Z. Deng, S. Han, T. Liu, N. Wen, W. Lu, X. Geng, S. Huang, Y. Jin, Tissue-engineered skin containing mesenchymal stem cells improves burn wounds, Artif. Organs 32 (2008) 925–931, https://doi.org/10.1111/j.1525-1594.2008.00654.x.

[2] S. Morelli, S. Salerno, H.M. Ahmed, A. Piscioneri, L. Bartolo, Recent strategies combining biomaterials and stem cells for bone, liver and skin regeneration, Curr. Stem Cell Res. Ther. 11 (2016) 676–691, https://doi.org/10.2174/1574888x11666160201120004.

[3] V. Falanga, S. Iwamoto, M. Chartier, T. Yufit, J. Butmarc, N. Kouttab, D. Shrayer, P. Carson, Autologous bone marrow-derived cultured mesenchymal stem cells delivered in a fibrin spray accelerate healing in murine and human cutaneous wounds, Tissue Eng. 13 (2007) 1299–1312, https://doi.org/10.1089/ten.2006.0278.

[4] E. Bey, M. Prat, P. Duhamel, M. Benderitter, M. Brachet, F. Trompier, P. Battaglini, I. Ernou, L. Boutin, M. Gourven, F. Tissedre, S. Créa, C.A. Mansour, T. de Revel, H. Carsin, P. Gourmelon, J.J. Lataillade, Emerging therapy for improving wound repair of severe radiation burns using local bone marrow-derived stem cell administrations, Wound Repair Regen. 18 (2010) 50–58, https://doi.org/10.1111/j.1524-475X.2009.00562.x.

[5] D.E. Lee, N. Ayoub, D.K. Agrawal, Mesenchymal stem cells and cutaneous wound healing: novel methods to increase cell delivery and therapeutic efficacy, Stem Cell Res. Ther. 7 (2016) 37, https://doi.org/10.1186/s13287-016-0303-6.

[6] R.K. Schneider, J. Anraths, R. Kramann, J. Bornemann, M. Bovi, R. Knüchel, S. Neuss, The role of biomaterials in the direction of mesenchymal stem cell properties and extracellular matrix remodelling in dermal tissue engineering, Biomaterials 31 (2010) 7948–7959, https://doi.org/10.1016/j.biomaterials.2010.07.003.

[7] R.E.B. Fitzsimmons, M.S. Mazurek, A. Soos, C.A. Simmons, Mesenchymal stromal/stem cells in regenerative medicine and tissue engineering, Stem Cell. Int. (2018) (2018) 8031718, https://doi.org/10.1155/2018/8031718.

[8] X. Jin, T. Lin, Y. Xu, Stem cell therapy and immunological rejection in animal models, Curr. Mol. Pharmacol. 9 (2016) 284–288, https://doi.org/10.2174/

187446720866615092815351l.
[9] J. Zhou, J. Zhang, L. Wu, F. Zhu, H. Xu, Tetramethylpyrazine/ligustrazine can improve the survival rate of adipose-derived stem cell transplantation, Ann. Plast. Surg. 84 (2020) 328–333, https://doi.org/10.1097/SAP.0000000000002146.
[10] D. Bhartiya, H. Patel, R. Ganguly, A. Shaikh, Y. Shukla, D. Sharma, P. Singh, Novel insights into adult and cancer stem cell biology, Stem Cell. Dev. 27 (2018) 1527–1539, https://doi.org/10.1089/scd.2018.0118.
[11] H.Y. Lee, I.S. Hong, Double-edged sword of mesenchymal stem cells: cancer-promoting versus therapeutic potential, Canc. Sci. 108 (2017) 1939–1946, https://doi.org/10.1111/cas.13334.
[12] N. Kalinina, D. Kharlampieva, M. Loguinova, I. Butenko, O. Pobeguts, A. Efimenko, L. Ageeva, G. Sharonov, D. Ischenko, D. Alekseev, O. Grigorieva, V. Sysoeva, K. Rubina, V. Lazarev, V. Govorun, Characterization of secretomes provides evidence for adipose-derived mesenchymal stromal cells subtypes, Stem Cell Res. Ther. 6 (2015) 221, https://doi.org/10.1186/s13287-015-0209-8.
[13] S.H. Bhang, S. Lee, J.Y. Shin, T.J. Lee, H.K. Jang, B.S. Kim, Efficacious and clinically relevant conditioned medium of human adipose-derived stem cells for therapeutic angiogenesis, Mol. Ther. 22 (2014) 862–872, https://doi.org/10.1038/mt.2013.301.
[14] T.P. Lozito, R.S. Tuan, Mesenchymal stem cells inhibit both endogenous and exogenous MMPs via secreted TIMPs, J. Cell. Physiol. 226 (2011) 385–396, https://doi.org/10.1002/jcp.22344.
[15] B. Mathew, S. Ravindran, X. Liu, L. Torres, M. Chennakesavalu, C.C. Huang, L. Feng, R. Zelka, J. Lopez, M. Sharma, S. Roth, Mesenchymal stem cell-derived extracellular vesicles and retinal ischemia-reperfusion, Biomaterials 197 (2019) 146–160, https://doi.org/10.1016/j.biomaterials.2019.01.016.
[16] J. Sun, Y. Zhang, X. Song, J. Zhu, Q. Zhu, The healing effects of conditioned medium derived from mesenchymal stem cells on radiation-induced skin wounds in rats, Cell Transplant. 28 (2019) 105–115, https://doi.org/10.1177/0963689718807410.
[17] M.H. Kim, W.H. Wu, J.H. Choi, J. Kim, J.H. Jun, Y. Ko, J.H. Lee, Galectin-1 from conditioned medium of three-dimensional culture of adipose-derived stem cells accelerates migration and proliferation of human keratinocytes and fibroblasts, Wound Repair Regen. 26 (Suppl 1) (2018) S9–S18, https://doi.org/10.1111/wrr.12579.
[18] E.K. Jun, Q. Zhang, B.S. Yoon, J.H. Moon, G. Lee, G. Park, P.J. Kang, J.H. Lee, A. Kim, S. You, Hypoxic conditioned medium from human amniotic fluid-derived mesenchymal stem cells accelerates skin wound healing through TGF-β/SMAD2 and PI3K/Akt pathways, Int. J. Mol. Sci. 15 (2014) 605–628, https://doi.org/10.3390/ijms15010605.
[19] R. Thomas, K.R. Soumya, J. Mathew, E.K. Radhakrishnan, Electrospun polycaprolactone membrane incorporated with biosynthesized silver nanoparticles as effective wound dressing material, Appl. Biochem. Biotechnol. 176 (2015) 2213–2224, https://doi.org/10.1007/s12010-015-1709-9.
[20] A. Greiner, J.H. Wendorff, Electrospinning: a fascinating method for the preparation of ultrathin fibers, Angew Chem. Int. Ed. Engl. 46 (2007) 5670–5703, https://doi.org/10.1002/anie.200604646.
[21] B.M. Min, G. Lee, S.H. Kim, Y.S. Nam, T.S. Lee, W.H. Park, Electrospinning of silk fibroin nanofibers and its effect on the adhesion and spreading of normal human keratinocytes and fibroblasts in vitro, Biomaterials 25 (2004) 1289–1297, https://doi.org/10.1016/j.biomaterials.2003.08.045.
[22] H. Jiang, Y. Hu, Y. Li, P. Zhao, K. Zhu, W. Chen, A facile technique to prepare biodegradable coaxial electrospun nanofibers for controlled release of bioactive agents, J. Contr. Release 108 (2005) 237–243, https://doi.org/10.1016/j.jconrel.2005.08.006.
[23] T.G. Kim, D.S. Lee, T.G. Park, Controlled protein release from electrospun biodegradable fiber mesh composed of poly(epsilon-caprolactone) and poly(ethylene oxide), Int. J. Pharm. 338 (2007) 276–283, https://doi.org/10.1016/j.ijpharm.2007.01.040.
[24] Y. Yang, X. Li, M. Qi, S. Zhou, J. Weng, Release pattern and structural integrity of lysozyme encapsulated in core-sheath structured poly(DL-lactide) ultrafine fibers prepared by emulsion electrospinning, Eur. J. Pharm. Biopharm. 69 (2008) 106–116, https://doi.org/10.1016/j.ejpb.2007.10.016.
[25] Y. Yang, T. Xia, W. Zhi, L. Wei, J. Weng, C. Zhang, X. Li, Promotion of skin regeneration in diabetic rats by electrospun core-sheath fibers loaded with basic fibroblast growth factor, Biomaterials 32 (2011) 4243–4254, https://doi.org/10.1016/j.biomaterials.2011.02.042.
[26] M. Arana, M. Mazo, P. Aranda, B. Pelacho, F. Prosper, Adipose tissue-derived mesenchymal stem cells: isolation, expansion, and characterization, Methods Mol. Biol. 1036 (2013) 47–61, https://doi.org/10.1007/978-1-62703-511-8_4.
[27] T. He, X. Bai, L. Yang, L. Fan, Y. Li, L. Su, J. Gao, S. Han, D. Hu, Loureirin B inhibits hypertrophic scar formation via inhibition of the TGF-beta1-ERK/JNK pathway, Cell. Physiol. Biochem. 37 (2015) 666–676, https://doi.org/10.1159/000430385.
[28] C. O'Fagain, K. Colliton, Storage and lyophilization of pure proteins, Methods Mol. Biol. 1485 (2017) 159–190, https://doi.org/10.1007/978-1-4939-6412-3_9.
[29] G. Xia, H. Zhang, R. Cheng, H. Wang, Z. Song, L. Deng, X. Huang, H.A. Santos, W. Cui, Localized controlled delivery of gemcitabine via microsol electrospun fibers to prevent pancreatic cancer recurrence, Adv. Healthc. Mater. 7 (2018) e1800593, , https://doi.org/10.1002/adhm.201800593.
[30] L. Wu, Y. Gu, L. Liu, J. Tang, J. Mao, K. Xi, Z. Jiang, Y. Zhou, Y. Xu, L. Deng, L. Chen, W. Cui, Hierarchical micro/nanofibrous membranes of sustained releasing VEGF for periosteal regeneration, Biomaterials 227 (2020) 119555, https://doi.org/10.1016/j.biomaterials.2019.119555.
[31] Y. Li, W. Zhang, J. Gao, J. Liu, H. Wang, J. Li, X. Yang, T. He, H. Guan, Z. Zheng, S. Han, M. Dong, J. Han, J. Shi, D. Hu, Adipose tissue-derived stem cells suppress hypertrophic scar fibrosis via the p38/MAPK signaling pathway, Stem Cell Res. Ther. 7 (2016) 102, https://doi.org/10.1186/s13287-016-0356-6.
[32] L.J. Green, H. Zhou, V. Padmanabhan, A. Shikanov, Adipose-derived stem cells promote survival, growth, and maturation of early-stage murine follicles, Stem Cell Res. Ther. 10 (2019) 102, https://doi.org/10.1186/s13287-019-1199-8.
[33] A.S. Maharaj, P.A. D'Amore, Roles for VEGF in the adult, Microvasc. Res. 74 (2007) 100–113, https://doi.org/10.1016/j.mvr.2007.03.004.
[34] T.K. Bhattacharyya, P. Jackson, M.K. Patel, J.R. Thomas, Epidermal cell proliferation in calorie-restricted aging rats, Curr. Aging Sci. 5 (2012) 96–104, https://doi.org/10.2174/1874609811205020096.
[35] P.A. Zuk, M. Zhu, P. Ashjian, D.A. De Ugarte, J.I. Huang, H. Mizuno, Z.C. Alfonso, J.K. Fraser, P. Benhaim, M.H. Hedrick, Human adipose tissue is a source of multipotent stem cells, Mol. Biol. Cell 13 (2002) 4279–4295, https://doi.org/10.1091/mbc.e02-02-0105.
[36] E.C. Jensen, Quantitative analysis of histological staining and fluorescence using ImageJ, Anat. Rec. 296 (2013) 378–381, https://doi.org/10.1002/ar.22641.
[37] F. Varghese, A.B. Bukhari, R. Malhotra, A. DeIHC Profiler, An open source plugin for the quantitative evaluation and automated scoring of immunohistochemistry images of human tissue samples, PloS One 9 (2014) e96801, , https://doi.org/10.1371/journal.pone.0096801.
[38] P.A. Zuk, M. Zhu, H. Mizuno, J. Huang, J.W. Futrell, A.J. Katz, P. Benhaim, H.P. Lorenz, M.H. Hedrick, Multilineage cells from human adipose tissue: implications for cell-based therapies, Tissue Eng. 7 (2001) 211–228, https://doi.org/10.1089/107632701300062859.
[39] S.A. Park, V.K. Raghunathan, N.M. Shah, L. Teixeira, M.J. Motta, J. Covert, R. Dubielzig, M. Schurr, R.R. Isseroff, N.L. Abbott, J. McAnulty, C.J. Murphy, PDGF-BB does not accelerate healing in diabetic mice with splinted skin wounds, PloS One 9 (2014) e104447, , https://doi.org/10.1371/journal.pone.0104447.
[40] X. Zhao, X. Sun, L. Yildirimer, Q. Lang, Z.Y.W. Lin, R. Zheng, Y. Zhang, W. Cui, N. Annabi, A. Khademhosseini, Cell infiltrative hydrogel fibrous scaffolds for accelerated wound healing, Acta Biomater. 49 (2017) 66–77, https://doi.org/10.1016/j.actbio.2016.11.017.
[41] S.H. Ranganath, O. Levy, M.S. Inamdar, J.M. Karp, Harnessing the mesenchymal stem cell secretome for the treatment of cardiovascular disease, Cell Stem Cell 10 (2012) 244–258, https://doi.org/10.1016/j.stem.2012.02.005.
[42] Y. Zhang, C. Deng, J. Qian, M. Zhang, X. Li, Improvement of radiotherapy-induced lacrimal gland injury by induced pluripotent stem cell-derived conditioned medium via MDK and inhibition of the p38/JNK pathway, Int. J. Mol. Sci. 15 (2014) 18407–18421, https://doi.org/10.3390/ijms151018407.
[43] Q.L. Loh, C. Choong, Three-dimensional scaffolds for tissue engineering applications: role of porosity and pore size, Tissue Eng. B Rev. 19 (2013) 485–502, https://doi.org/10.1089/ten.TEB.2012.0437.
[44] M. Bernard, E. Jubeli, M.D. Pungente, N. Yagoubi, Biocompatibility of polymer-based biomaterials and medical devices - regulations, in vitro screening and risk-management, Biomater. Sci. 6 (2018) 2025–2053, https://doi.org/10.1039/c8bm00518d.
[45] S. Kuttappan, D. Mathew, J.I. Jo, R. Tanaka, D. Menon, T. Ishimoto, T. Nakano, S.V. Nair, M.B. Nair, Y. Tabata, Dual release of growth factor from nanocomposite fibrous scaffold promotes vascularisation and bone regeneration in rat critical sized calvarial defect, Acta Biomater. 78 (2018) 36–47, https://doi.org/10.1016/j.actbio.2018.07.050.
[46] M. Kabiri, S. Oraee-Yazdani, M. Dodel, H. Hanaee-Ahvaz, S. Soudi, E. Seyedjafari, M. Salehi, M. Soleimani, Cytocompatibility of a conductive nanofibrous carbon nanotube/poly (L-Lactic acid) composite scaffold intended for nerve tissue engineering, EXCLI J. 14 (2015) 851–860, https://doi.org/10.17179/excli2015-282.
[47] M. Xue, C.J. Jackson, Extracellular matrix reorganization during wound healing and its impact on abnormal scarring, Adv. Wound Care 4 (2015) 119–136, https://doi.org/10.1089/wound.2013.0485.
[48] J.K. Fraser, I. Wulur, Z. Alfonso, M.H. Hedrick, Fat tissue: an underappreciated source of stem cells for biotechnology, Trends Biotechnol. 24 (2006) 150–154, https://doi.org/10.1016/j.tibtech.2006.01.010.
[49] J.M. Gimble, F. Guilak, B.A. Bunnell, Clinical and preclinical translation of cell-based therapies using adipose tissue-derived cells, Stem Cell Res. Ther. 1 (2010) 19, https://doi.org/10.1186/scrt19.
[50] J.M. Gimble, A.J. Katz, B.A. Bunnell, Adipose-derived stem cells for regenerative medicine, Circ. Res. 100 (2007) 1249–1260, https://doi.org/10.1161/01.RES.0000265074.83288.09.
[51] Y. Lee, S. El Andaloussi, M.J. Wood, Exosomes and microvesicles: extracellular vesicles for genetic information transfer and gene therapy, Hum. Mol. Genet. 21 (2012) R125–R134, https://doi.org/10.1093/hmg/dds317.
[52] J. Wu, Y. Wang, L. Li, Functional significance of exosomes applied in sepsis: a novel approach to therapy, Biochim. Biophys. Acta (BBA) - Mol. Basis Dis. 1863 (2017) 292–297, https://doi.org/10.1016/j.bbadis.2016.10.024.
[53] D.G. Phinney, M.F. Pittenger, Concise review: MSC-derived exosomes for cell-free therapy, Stem Cell. 35 (2017) 851–858.
[54] A.I. Caplan, D. Correa, The MSC: an injury drugstore, Cell stem cell 9 (2011) 11–15, https://doi.org/10.1002/stem.2575.
[55] G. Sagaradze, O. Grigorieva, P. Nimiritsky, N. Basalova, N. Kalinina, Z. Akopyan, A. Efimenko, Conditioned medium from human mesenchymal stromal cells: towards the clinical translation, Int. J. Mol. Sci. 20 (2019) 1656, https://doi.org/10.3390/ijms20071656.
[56] A. Amouzegar, S.K. Chauhan, Effector and regulatory T cell trafficking in corneal allograft rejection, Mediat. Inflamm. (2017) (2017) 8670280, https://doi.org/10.1155/2017/8670280.
[57] C.J. Hoornaert, D. Le Blon, A. Quarta, J. Daans, H. Goossens, Z. Berneman, P. Ponsaerts, Concise review: innate and adaptive immune recognition of allogeneic and xenogeneic cell transplants in the central nervous system, Stem Cells Transl. Med. 6 (2017) 1434–1441, https://doi.org/10.1002/sctm.16-0434.

[58] S.H. Lee, S.Y. Jin, J.S. Song, K.K. Seo, K.H. Cho, Paracrine effects of adipose-derived stem cells on keratinocytes and dermal fibroblasts, Ann. Dermatol. 24 (2012) 136–143, https://doi.org/10.5021/ad.2012.24.2.136.
[59] C. Kichenbrand, E. Velot, P. Menu, V. Moby, Dental pulp stem cell-derived conditioned medium: an attractive alternative for regenerative therapy, Tissue Eng. B Rev. 25 (2019) 78–88, https://doi.org/10.1089/ten.TEB.2018.0168.
[60] K.I. Izutsu, Applications of freezing and freeze-drying in pharmaceutical formulations, Adv. Exp. Med. Biol. 1081 (2018) 371–383, https://doi.org/10.1007/978-981-13-1244-1_20.
[61] Z. Wang, Y. Qian, L. Li, L. Pan, L.W. Njunge, L. Dong, L. Yang, Evaluation of emulsion electrospun polycaprolactone/hyaluronan/epidermal growth factor nanofibrous scaffolds for wound healing, J. Biomater. Appl. 30 (2016) 686–698, https://doi.org/10.1177/0885328215586907.
[62] P. Peh, N.S. Lim, A. Blocki, S.M. Chee, H.C. Park, S. Liao, C. Chan, M. Raghunath, Simultaneous delivery of highly diverse bioactive compounds from blend electrospun fibers for skin wound healing, Bioconjugate Chem. 26 (2015) 1348–1358, https://doi.org/10.1021/acs.bioconjchem.5b00123.
[63] A.L. Rippa, E.P. Kalabusheva, E.A. Vorotelyak, Regeneration of dermis: scarring and cells involved, Cells 8 (2019) 607, https://doi.org/10.3390/cells8060607.
[64] J.M. Reinke, H. Sorg, Wound repair and regeneration, Eur. Surg. Res. 49 (2012) 35–43, https://doi.org/10.1159/000339613.
[65] P. Ault, A. Plaza, J. Paratz, Scar massage for hypertrophic burns scarring-a systematic review, Burns 44 (2018) 24–38, https://doi.org/10.1016/j.burns.2017.05.006.
[66] B.C. Brown, S.P. McKenna, K. Siddhi, D.A. McGrouther, A. Bayat, The hidden cost of skin scars: quality of life after skin scarring, J. Plast. Reconstr. Aesthetic Surg. 61 (2008) 1049–1058, https://doi.org/10.1016/j.bjps.2008.03.020.
[67] J. Zhang, Y. Li, X. Bai, Y. Li, J. Shi, D. Hu, Recent advances in hypertrophic scar, Histol. Histopathol. 33 (2018) 27–39, https://doi.org/10.14670/HH-11-908.